Bending Stress in Plant Stems: Models and Assumptions

Christopher J. Stubbs, Navajit S. Baban, Daniel J. Robertson, Loay Alzube and Douglas D. Cook

Abstract Analytic expressions for bending stress can be used to predict mechanical stresses and failure of plant stems. However, the nonuniform shape and anisotropic material properties of plant stems contradict several assumptions that are typically used in the derivation of bending stress equations. The purpose of this chapter is to analyze each of these assumptions to determine the accuracy with which beam theory can predict stresses in plant stems. Finite element models of plant stems were used to investigate and quantify the effect of each assumption. Finally, experimental case-study data was used to illustrate the applications of these equations. The goal of this work is to enable researchers to make informed decisions regarding mechanical models of plant stems used to predict of measure mechanical behavior of plants and plant tissues.

Keywords Plant stems · Stress · Modeling · Assumptions · Bending · Beams Maize

Introduction

Plant stems typically fail due to bending loads. When a failure occurs, it typically manifests in one of the four modes: buckling or kinking, splitting along longitudinal fibers, compressive tissue collapse, or tensile fracture of the stem tissue (Wegst and Ashby 2007). This chapter focuses on the techniques for modeling tensile, com-

N. S. Baban · L. Alzube · D. D. Cook (✉)
New York University, Abu Dhabi Campus, PO BOX 129188, Abu Dhabi, United Arab Emirates
e-mail: douglascook@nyu.edu

D. D. Cook
Brigham Young University, Provo, UT 84602, USA

D. J. Robertson
University of Idaho, 875 Perimeter Drive, Gauss-Johnson 234 G, Idaho, MS 0902, USA

C. J. Stubbs
New York University, 6 MetroTech Center, Brooklyn, NY 11201, USA

A. Geitmann and J. Gril (eds.), *Plant Biomechanics*,
https://doi.org/10.1007/978-3-319-79099-2_3

pressive, and shear stresses within the stem, which are responsible for the latter two failure modes.

Equations from engineering beam theory are frequently used to predict mechanical stresses that occur in plant stems due to external loading. Beam theory has been applied to studies on the thigmomorphogenesis of tomato stems (Coutand et al. 2000), the mechanics of tree trunks, (Dean and Long 1986; Speck et al. 1990), flexural strength of crops (Kokubo et al. 1989), and plant growth mechanisms such as gravitropism (Zandomeni and Schopfer 1994). More detailed information about bending stress equations are available in books such as *Plant Biomechanics* (Niklas 1992), *Plant Physics* (Niklas and Spatz 2012), and in the engineering literature (Beer et al. 2012; Boresi and Schmidt 2003; Crandall 2012; Timoshenko 1940).

In each of these books, certain assumptions are required to arrive at a set of equations describing structural stresses under bending. These assumptions are typically made as a means to an end, with the focus being on the final equations. But Karl Niklas alluded to a deeper understanding in the preface to *Plant Biomechanics* (Niklas 1992). He stated that the purpose of that book was "to illustrate representative principles rather than to delve deeply into them." The purpose of this chapter is to undertake the deeper work referred to by Niklas by dissecting and evaluating the derivation process in order to provide the reader with a clearer understanding of the accuracy and limitations of bending stress equations as applied to plant stems.

The chapter consists of several sections. Bending stress equations are derived in section "Derivation of Bending Stress Equations" using a relatively small set of assumptions. This section gives an explicit mathematical definition of each assumption used in the derivation process. Alternative formulations are also provided where traditional assumptions are not appropriate for the modeling of plant stems. In section "Evaluating Model Assumptions", the validity of each assumption made during the derivation is investigated by comparing analytic results with those obtained from a finite element model. Section "Structural Characteristics of Plant Stems" addresses structural aspects of the plant stems that are not explicitly addressed within the modeling assumptions. Section "Case Studies" provides several experimental case studies in which bending equations were applied to plant stems. Finally, the chapter concludes with section "Summary and Future Work": a brief summary of the chapter and identification of areas in which further work is needed.

Background Information

To aid the reader, several essential terms and concepts will be briefly defined and described before proceeding with the derivation of bending equations. Table 1 provides a list of terms, symbols, and nomenclature.

When an external force is applied to a plant stem, internal stresses develop within the stem to resist the externally applied load. These stresses act in addition to internal stresses that may be present in the absence of external loading (i.e., residual internal stresses Archer 1987; Vandiver and Goriely 2009). Mechanical stresses can be

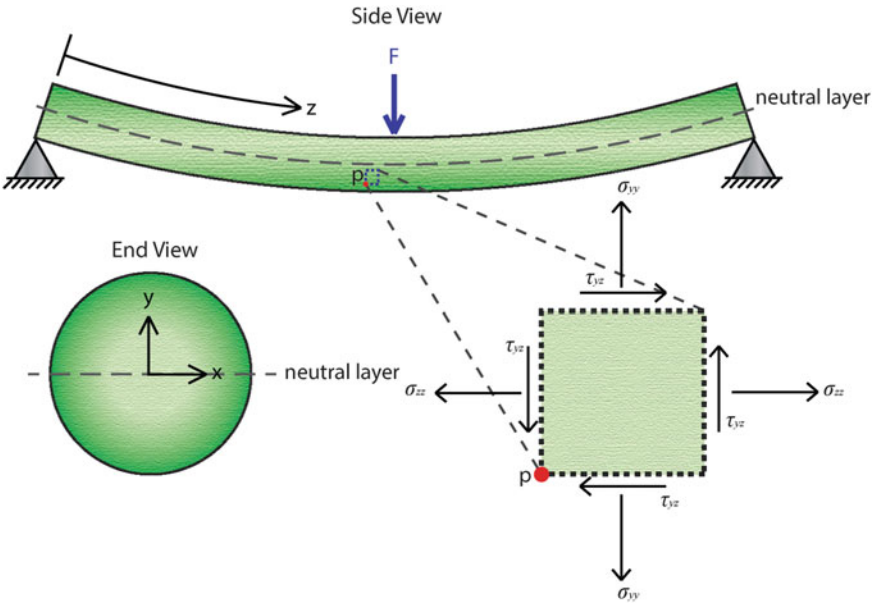

Fig. 1 An infinitesimally small cube with unit thickness taken within the plant stem under three-point bending used to quantify the stresses at a point P

characterized into two general categories: normal stresses and shear stresses. Normal stresses act perpendicular to the surface of interest and cause tension or compression. Shear stresses act parallel to the surface of interest. They do not induce tension or compression but cause shear deformation or torsion.

When an external load causes a plant stem to bend, internal normal and shear stresses are developed in the plant tissue. In this chapter, bending loads will primarily be illustrated using the common three-point bending load configuration depicted in Fig. 1. As shown in this figure, the top of the beam will be compressed and bottom of the beam will be stretched. Thus, the top of the beam will experience normal compressive stresses, while the bottom of the beam experiences normal tensile stresses. The normal stress changes linearly from maximum compressive stress at the top of the beam, to maximum tensile stress at the bottom of the beam (Byars et al. 1983). The location inside the beam at which the normal stress changes from compressive to tensile is termed as the neutral layer. The neutral layer is neither stretched nor compressed, thus the normal stress at this layer is equal to zero. The neutral layer is typically, though not always located at or near the geometric centroid of the stem (Boresi and Schmidt 2003; Niklas 1992). Methods for determining the precise location of the neutral layer are beyond the scope of this study, but are available in the literature (Boresi and Schmidt 2003).

Table 1 Terminology and symbols used within this chapter

Symbol(s) or Terms	Description
x, y, z	Cartesian coordinates. The z axis is aligned with the apical–basal direction of the stem. The x and y coordinates originate from the geometric cross section of the plant stem (see Fig. 1)
L	Length
D	Diameter of the plant stem
σ_{ii}	Normal stresses in the i direction
ε_i	Normal strain in the i direction
τ_{ij}	Shear stress on the i face, in the j direction
ρ	Radius of the curvature
E_i	Stiffness (Young's Modulus) in the i direction
G_{ij}	Shear modulus between the i direction and j direction
V	Internal shear load
M	Internal bending moment
I	Area moment of inertia
w(y)	Width of the cross section as a function of y coordinates
I_E	Material stiffness weighted second moment of area
σ_1, σ_2	Principal normal stresses
σ_v	von Mises stress
[ε]	Strain matrix
[K]	Stiffness matrix
[σ]	Stress matrix
S_{rind}	Section modulus of the rind
ν_{ij}	Poisson's ratio between the i and j directions
Beam	A slender structure that is primarily subjected to transverse loading (Riley and Zachary 1989)
Neutral layer	The layer in a beam where the axial stress is zero. This layer corresponds with $y=0$
Sample slenderness (L/D)	Ratio of beam's length to its diameter (or height)
Diameter distance	The nondimensional distance from a support or load to a point of measurement, measured in terms of the number of stem diameters
Isotropy	A material which has the same properties in every direction (Callister and Rethwisch 2012)
Anisotropy	Material which has different material properties in different directions (Callister and Rethwisch 2012)
Orthotropy	Material that possesses material symmetry along orthogonal axes (e.g., wood) (Shukla et al. 1989)

Table 2 List of assumptions used to derive bending stress equations

Assumptions	
A	Orthotropic linear elasticity (Eq. 1)
B	Normal stress σ_{zz} is much larger than σ_{xx} & σ_{yy} (Eq. 2)
C	Bending is locally approximated by an arc (Eq. 3)
D	Homogeneous cross-sectional stiffness (no equation)
E	Shear stress τ_{yz} is much larger than shear stresses τ_{xz} & τ_{xy} (Eq. 11)
F	Shear stress is a function of y only (Eq. 11)

Derivation of Bending Stress Equations

Many sources that describe the derivation of bending stress equations introduce more assumptions than are actually necessary. The derivation in this chapter utilizes just 6 assumptions, which are briefly described in Table 2. As mentioned previously, the validity of each assumption will be evaluated in section "Evaluating Model Assumptions" along with the effect each assumption has on the accuracy of the bending equations.

Normal Stresses

We begin by assuming plant tissue can be modeled using a three-dimensional, orthotropic, linear elastic material (Assumption A). This type of material model is often used to describe the properties of wood and other fibrous composites and is, therefore, a good approximation of plant tissue (Agarwal et al. 2006; Niklas 1992; Shukla et al. 1989). Orthotropic, linear elastic material theory states that material strains are the product of a compliance matrix and a stress vector as shown below (refer to Table 1 for the interpretation of subscripts).

$$\begin{bmatrix} \varepsilon_{xx} \\ \varepsilon_{yy} \\ \varepsilon_{zz} \\ \varepsilon_{yz} \\ \varepsilon_{zx} \\ \varepsilon_{xy} \end{bmatrix} = \begin{bmatrix} \frac{1}{E_x} & -\frac{v_{yx}}{E_y} & -\frac{v_{zx}}{E_z} & 0 & 0 & 0 \\ -\frac{v_{xy}}{E_x} & \frac{1}{E_y} & -\frac{v_{zy}}{E_z} & 0 & 0 & 0 \\ -\frac{v_{xz}}{E_x} & -\frac{v_{yz}}{E_y} & \frac{1}{E_z} & 0 & 0 & 0 \\ 0 & 0 & 0 & \frac{1}{2G_{yz}} & 0 & 0 \\ 0 & 0 & 0 & 0 & \frac{1}{2G_{zx}} & 0 \\ 0 & 0 & 0 & 0 & 0 & \frac{1}{2G_{xy}} \end{bmatrix} \begin{bmatrix} \sigma_{xx} \\ \sigma_{yy} \\ \sigma_{zz} \\ \sigma_{yz} \\ \sigma_{zx} \\ \sigma_{xy} \end{bmatrix} \quad (1)$$

Next, we assume normal stresses in the z direction are much larger than the normal stresses in the x and y directions (Assumption B). The accuracy of this assumption primarily depends upon local slenderness (see section "Evaluating Model Assumptions"). If σ_{xx} and σ_{yy}, are neglected, and, therefore, assumed to be zero, Eq. 1 reduces to a much simpler form:

$$\sigma_{zz} = E_z \varepsilon_{zz}, \tag{2}$$

Next, we assume that local deformation of a plant stem in bending can be approximated by an arc (Assumption C). Under this assumption, the strain is inversely proportional to local arc radius (ρ) and is linearly related to distance from the neutral layer (y). In other words, tensile and compressive normal forces occur on opposing sides of the neutral layer and smaller arc radii induce larger strains than bigger arc radii. The assumption is stated mathematically by the following equation:

$$\varepsilon_{zz} = \frac{y}{\rho} \tag{3}$$

Combining Eq. 2 and Assumption C, we have the following:

$$\sigma_{zz} = E_{zz} \frac{y}{\rho} \tag{4}$$

By Newton's first law, the total internal moment, *M,* of each cross section must be equal to the bending moment created by internal normal forces. Thus, at each point in the stem cross-section, the internal moment with respect to the neutral layer is equal to the sum of all internal normal forces multiplied by their distance from the neutral layer. Mathematically,

$$M = \int_A y \, \sigma_{zz} \, dA \tag{5}$$

Substituting Eq. 4 into Eq. 5 we have the following:

$$M = \int y \left(E_z \frac{y}{\rho} \right) dA \tag{6}$$

At this point, E_z is assumed to be constant across the cross section (Assumption D) and can, therefore, be placed outside of the integral. This is the first assumption which appears to be inappropriate for plant stems. Many plant stems, particularly grasses, utilize stiffness gradients to optimize structural integrity (Rüggeberg et al. 2008; Speck and Burgert 2011). Assumption D is used at this point to illustrate the traditional formulation and is later eliminated. Carrying on with an assumption of constant stiffness we obtain:

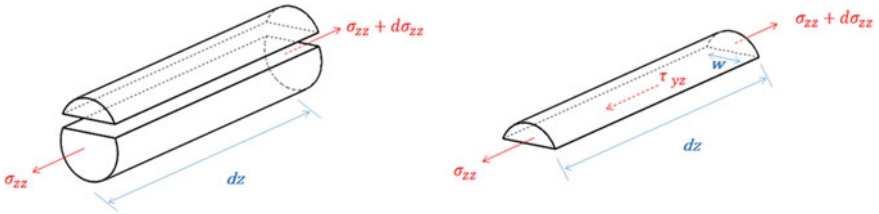

Fig. 2 Free-body diagrams of the differential segment of the plant stem showing the generation of shear stress due to changing normal stress along the longitudinal direction. The differential section sliced along a horizontal plane (left); the upper section in isolation (right)

$$M = \frac{E_z}{\rho} \int_A y^2 dA. \tag{7}$$

The integral term in Eq. 9 is recognized as the area moment of inertia (I):

$$I = \int_A y^2 dA \tag{8}$$

Thus, the internal bending moment depends upon material properties, area moment of inertia, and radius of curvature:

$$M = \frac{E_z I}{\rho} \tag{9}$$

Solving for the radius of curvature, ρ from Eq. 4 and substituting into Eq. 9 we find that the material effect is canceled yielding the classic equation for stress as a function of the internal bending moment, distance from the neutral layer, and area moment of inertia:

$$\sigma_{zz} = \frac{M\, y}{I} \tag{10}$$

Shear Stresses

None of the assumptions made thus far prohibit variation in the internal bending moment and normal stresses, σ_{zz}, along the longitudinal axis (z direction) of the stem. When internal normal stresses do vary along the length of the stem additional stress components are required to achieve internal static equilibrium. The magnitude of these stresses can be determined by creating a free body diagram of a small region of excised tissue (Fig. 2).

Next, we assume that shear stress τ_{yz} is much larger than shear stresses τ_{xz} and τ_{xy} (Assumption E). Furthermore, we assume τ_{yz} does not vary in the x direction (Assumption F). Thus, τ_{yz} becomes a function only of y. When the τ_{yz} shear stress varies only in the y direction, the free body diagram of Fig. 2 can be used to determine the value of shear stresses by summing forces in the z direction.

The net force in the z direction due to normal stress, σ_{zz}, is the differential increase in σ_{zz}, integrated across xy cross section. This is the term on the right-hand side of Eq. 11. The net normal force is balanced by the net shear force, which is the integral of τ_{yz} across the horizontal plane. Since the shear stress is assumed to only vary in y, the integral reduces to the shear stress times the width as a function of, $w(y)$, which is the left-hand side of Eq. 11. The limits of the integration y_i and y_f denote y direction distances from the neutral layer to the considered and the outermost layer respectively.

$$\tau_{yz} w(y) dz = \int_{y_i}^{y_f} d\sigma_{zz} \cdot dA \tag{11}$$

Solving for the shear stress we have the following:

$$\tau_{yz} = \frac{1}{w(y)} \int_{y_i}^{y_f} \frac{d\sigma_{zz}}{dz} \cdot dA \tag{12}$$

Equation 10 can be substituted into Eq. 12 to obtain following equation:

$$\tau_{yz} = \frac{1}{w(y)} \int_{y_i}^{y_f} \frac{d}{dz} \left(\frac{M(z)y}{I} \right) \cdot dA \tag{13}$$

Because the derivative of the internal bending moment is equal to the internal shear, *v(z)* (Beer et al. 2012), a simplified form is obtained:

$$\tau_{yz} = \frac{V(z)}{I\, w(y)} \int_{y_i}^{y_f} y\, dA \tag{14}$$

For illustrative simplicity, if we assume a *rectangular* cross section, the width as a function of y becomes a simple constant and the shear stress is found as a function of y for a given value of z:

$$\tau_{yz} = \frac{V(z)}{I} \left(\frac{h^2}{8} - \frac{y^2}{2} \right) \tag{15}$$

This parabolic distribution of shear stress is the classic solution presented in most engineering textbooks, but because it required an assumption of the rectangular cross section, it is not appropriate for plant stems.

Adjusted Bending and Shear Stress Equations

Bending Stresses

Not all assumptions used in the previous derivation are valid for plant stems. The most erroneous assumption in Table 1 is constant cross-sectional stiffness (Assumption D). While some woody plants may be approximated as having a constant cross-sectional stiffness, this is not generally true (Niklas 1992). Instead of assuming that E_z is constant, we more accurately model a plant stem by assuming that stiffness varies as a function of y and x. Equation 7 is then rewritten as:

$$M = \int_A y \left(E_z(x, y) \frac{y}{\rho} \right) dA \tag{16}$$

We can remove ρ from the integral because it is constant in the plane of integration. After doing so, we define a new quantity: the material-weighted area moment of inertia. It is analogous to the traditional area moment of inertia, but each differential element dA is weighted by the material stiffness, E_z (x, y):

$$I_E = \int_A E_z(x, y)\, y^2\, dA \tag{17}$$

We now progress as before, with

$$M = \frac{I_E}{\rho} = \frac{I_E}{E_z(x, y)\frac{y}{\sigma}} \tag{18}$$

and finally,

$$\sigma = \frac{M\, E_z(x, y) y}{I_E} \tag{19}$$

When variable stiffness is considered, we see that the material stiffness remains in the equation for bending stress, thus leading to a slightly modified form of the traditional equation. As in the traditional form, I_E, and M act as a scaling constant in the determination of stress. Both of these terms affect the stress magnitude, but do not affect the spatial distribution of stress. The spatial stress distribution is found to be the first moment material stiffness about the stem's neutral layer: E_z $(x, y)y$.

Shear Stresses

A similar process can be followed to obtain shear stress for variable cross-sectional stiffness. By assuming E_z to be a function of x and y:

$$\tau_{yz} = \frac{1}{w(y)} \int_{y_i}^{y_f} \frac{d}{dz} \left(\frac{M(z)\, E(x, y)\, y}{I_E} \right) \cdot dA \tag{20}$$

By using Eq. 2, the above equation simplifies to

$$\tau_{yz} = \frac{V(z)}{I_E\, w(y)} \int_{y_i}^{y_f} E(x, y)\ y\ dA \tag{21}$$

Combined Stress States

Cartesian stresses provide mathematical convenience, but have certain limitations. For structures involving multiple stress components, the stresses responsible for failure are rarely aligned with the Cartesian axes. Three common methods for predicting failure stresses are principal stresses, maximum shear stress, and von Mises stresses. Readers that are not familiar with these terms may refer to *Advanced Mechanics of Materials* (Boresi and Schmidt 2003). A brief explanation of principal stresses and von Mises stresses are given below.

For two-dimensional stress states, any combination of σ_{zz} and τ_{yz} are equivalent to two principal normal stresses, σ_1 and σ_2 which are (a) invariant (i.e., independent of Cartesian coordinate orientation) and (b) orthogonal to each other (Beer et al. 2012). A state of pure stress, τ_{max} also exists for every stress state. For the two-dimensional bending stress states described above, the two principal normal stress (σ_1 and σ_2) can be obtained by the following relation (Beer et al. 2012):

$$\sigma_1\,,\ \sigma_2 = \frac{\sigma_{zz}}{2} \pm \sqrt{\frac{\sigma_{zz}^2}{4} + \tau_{yz}^2} \tag{22}$$

Maximum shear stress can be obtained by the following relation (Beer et al. 2012):

$$\tau_{\max} = \sqrt{\frac{\sigma_{zz}^2}{4} + \tau_{yz}^2} \tag{23}$$

Angle between σ_{zz} and σ_1 can be obtained by the following relation (Beer et al. 2012):

$$\tan(2\theta) = \frac{2\tau_{yz}}{\sigma_{xx}} \tag{24}$$

The maximum shear stress is always oriented at a 45° angle from the principal stresses.

Another common method for combining stresses is the von Mises failure criterion. For the two-dimensional bending stresses derived above, von Mises stress is given as (Beer et al. 2012):

$$\sigma_v = \sqrt{\sigma_{zz}^2 + 3\,\tau_{yz}^2} \tag{25}$$

These stresses provide a means of assessing total stress that is independent of the choice of coordinate system.

Evaluating Model Assumptions

We now proceed to analyze each assumption used in section "Derivation of Bending Stress Equations". In particular, the stresses predicted by the equations developed in section "Derivation of Bending Stress Equations" will be compared to stresses derived from a computational finite element model of a plant stem. A finite element model is used by the authors because finite element methods allow for a generalized strain and stress solution based on internal potential energy minimization, and therefore do not inherently rely on any of the assumptions made in section "Derivation of Bending Stress Equations" (Kim and Sankar 2009). Finite element modeling also enables parameterization of individual assumptions, loading conditions, and boundary conditions.

In the current work, all finite models of plant stems possessed circular cross sections. Both solid and hollow cross sections were analyzed. Hollow models did not include nodes. In general, discrepancies between the analytic equations of section "Derivation of Bending Stress Equations" and the solid cross-section finite element model were smaller than discrepancies between the analytic equations and the hollow cross-section finite element model. To provide conservative assessments of assumption validity, many results below only show comparisons with the hollow cross-section finite element model. A complete description of each finite element model can be found at the end of this chapter.

Assumption A: Material Model

Both the analytic equations of section "Derivation of Bending Stress Equations" and the finite element models presented in this section assume linearly elastic, transversely isotropic material properties. Although alternatives to this approach are pos-

sible, such formulations are beyond the scope of this chapter. In addition, all finite element models developed as part of this work possessed material stiffness in the z direction was 20 times higher than the material stiffness in the x and y directions (Gibson 2012).

Assumption (B): Negligible Normal Stresses in the x *and* y *Directions*

Assumption (B) dictates that the stress state of the stem is dominated by normal stress in the z direction (σ_{zz}). A comparison of the stresses predicted by the analytic bending equations and the finite element model is provided in Fig. 3. Because normal stress (σ_{zz}) increases linearly along the stem, each stress component was normalized by σ_{zz}. As shown in Fig. 3, the analytic model predicts two stress components, while the finite element model predicts all six stress components. As seen in the right-hand side of the figure, stress components σ_{xx}, σ_{yy}, and τ_{xy} reduce to less than 0.1% of the bending stress within two diameters of the support ($z/D < 2$), and within one diameter ($z/D < 1$) of the point of loading. In the span where σ_x, σ_y, and τ_{xy} are not depicted along the bottom edge of the chart ($2 < z/D < 24$), their values are much less than 0.1% of the bending stress. This measure is referred to as *diameter distance*, defined as the distance from a support or load point divided by the stem diameter, and will be discussed further in the following sections. Shear stresses τ_{yz} and τ_{xz} remain significant throughout, but reduce to below 10% of the bending stress at five diameters from the support. The shear components will be discussed in more detail later in this section.

Assumptions (C): Normal Strains Approximated by an Arc

The analytical stress equations assume that normal strains are linearly distributed about the neutral layer, and inversely proportional to the radius of curvature (Assumption C). The validity of this assumption was checked by examining the stress distributions in the xy-plane of both the hollow and the solid finite element model. Figure 4 shows the distribution of σ_{zz} predicted by the bending equations as well as the σ_{zz} distribution for the finite element model.

Figure 4 provides a comparison of normal stresses for a single cross section. A broader assessment of Assumption C is possible by examining the validity of this assumption as a function of diameter distance. If Assumption C is valid, each planar cross section of the stem will remain planar as the stem bends. Many textbooks use the phrase “plane sections remain plane” to describe this phenomenon (Bauchau and Craig 2009).

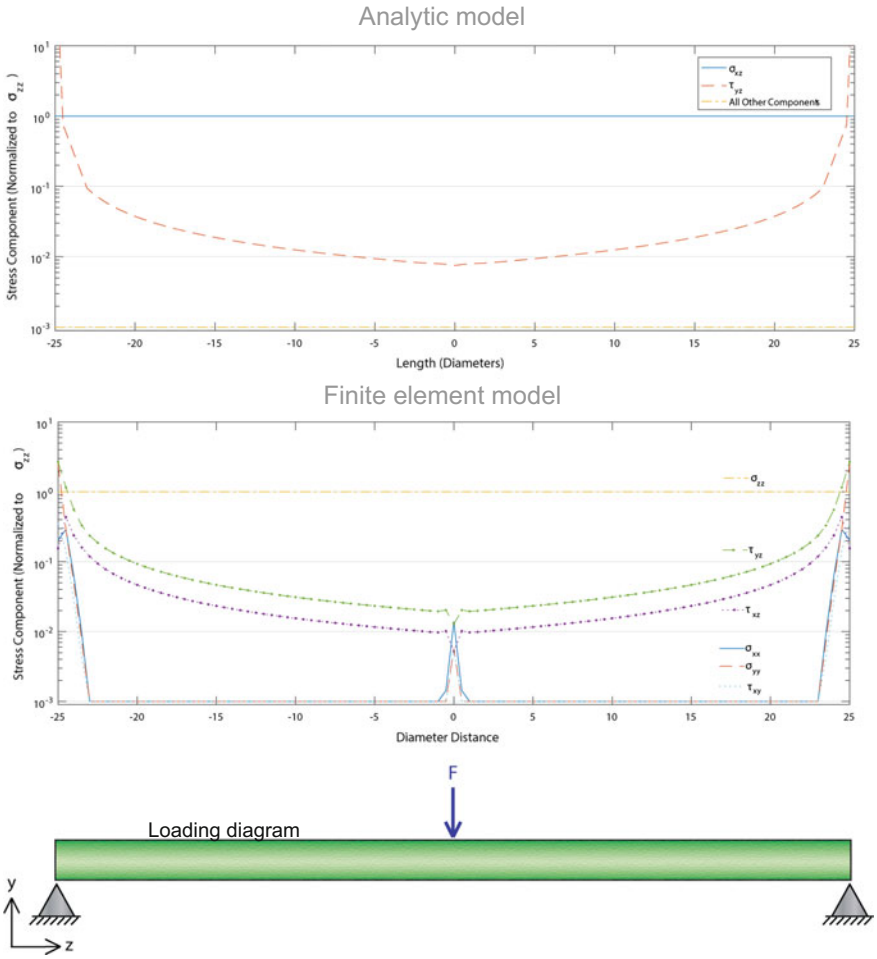

Fig. 3 Comparison of the stresses predicted by analytic bending equations (top) and the finite element model (middle). Both models are based on modeling a hollow circular cross section. Stresses have been normalized to σ_{zz}. All distances are measured in terms of diameters from the point of loading. For convenience, a loading diagram is provided at the bottom of the figure

Figure 5 illustrates the "nonplanarity" as a function of diameter distance based on data from the finite element model. Nonplanarity is defined as the maximum deviation from planar deformation, divided by the maximum deformation within the same plane. A nonplanarity value of zero thus implies perfectly planar deformation, while a nonplanarity value of 0.1 would imply that the maximum out-of-plane deformation is one-tenth of the maximum deformation of the same plane.

Out-of-plane deformation is directly related to the ratio between shear stresses and σ_{zz}. When σ_{zz} dominates, plane sections remain plane. This assumption is also

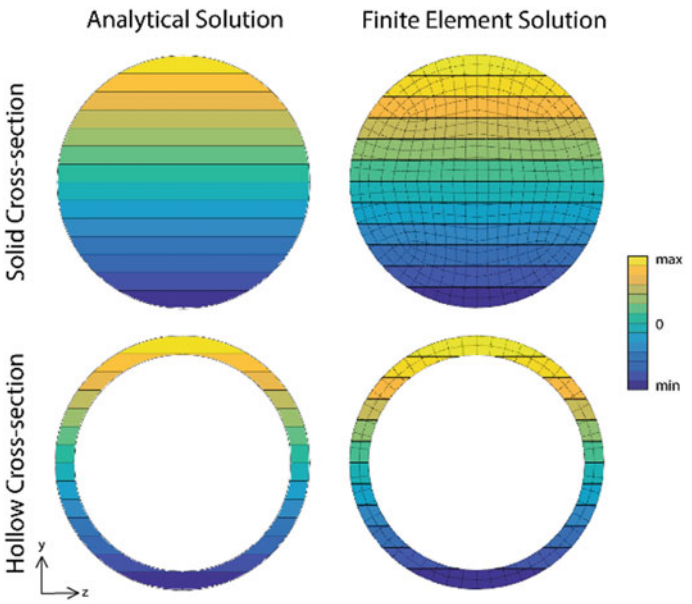

Fig. 4 Validation of assumption C. Bending stress distributions for a solid and hollow cross section, for the analytical solution (left) and finite element model (right)

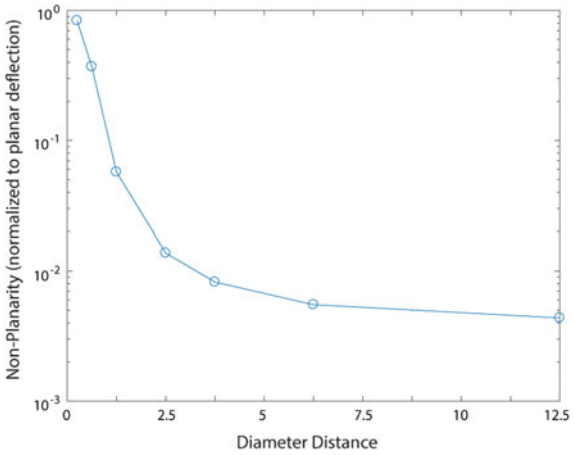

Fig. 5 Nonplanarity as a function of diameter distance from the point of loading. Non-planarity is defined as the maximum deviation from planarity divided by the maximum planar deformation of the cross-section

related to the diameter distance of the plant stem. For positions above 5 diameters from the left support, non-planarity is significantly less than 1%.

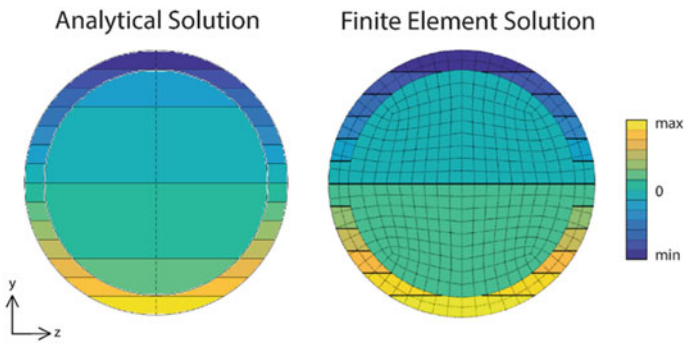

Fig. 6 Bending stress in a two-material cross section, analytical model (left) using Eq. 19 and the finite element model (right)

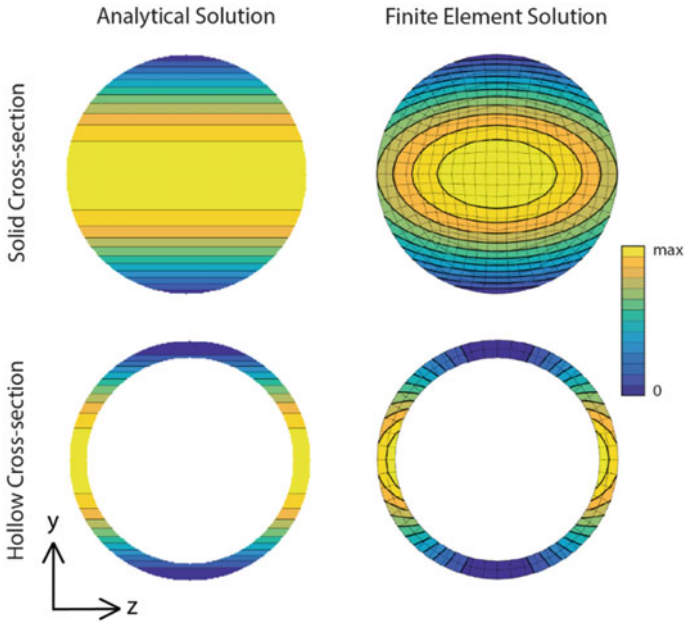

Fig. 7 Shear stress distributions for solid and hollow models of plant stems for τ_{yz}. Analytical model (left) using uniform cross-sectional stiffness and the finite element model (right)

Assumption (D): Constant Material Properties

Assumption (D) is that the stem is made of a single homogenous material. This assumption is not valid for most plant stems. Equation 19, utilizes the material-weighted area moment of inertia, which incorporates varying material properties for the calculation of bending stress. This generalized formula can be accurately used

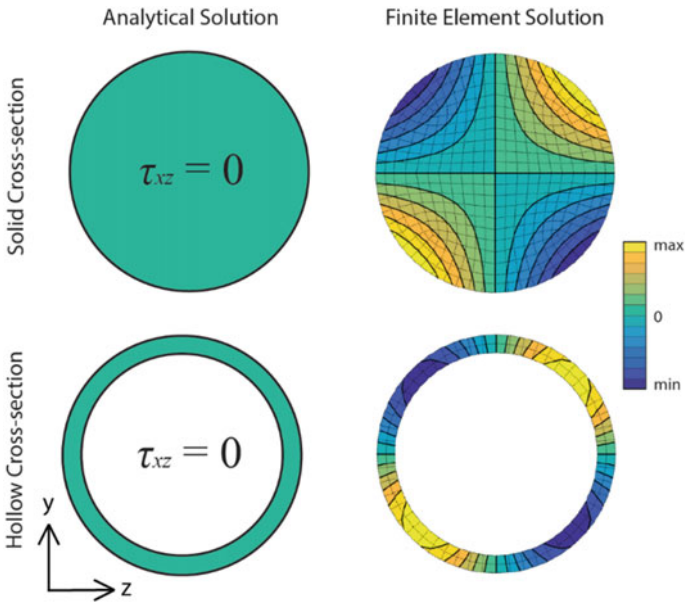

Fig. 8 Stress distributions for solid and hollow models of plant stems for τ_{xz}. Analytical model (left) and the finite element model (right)

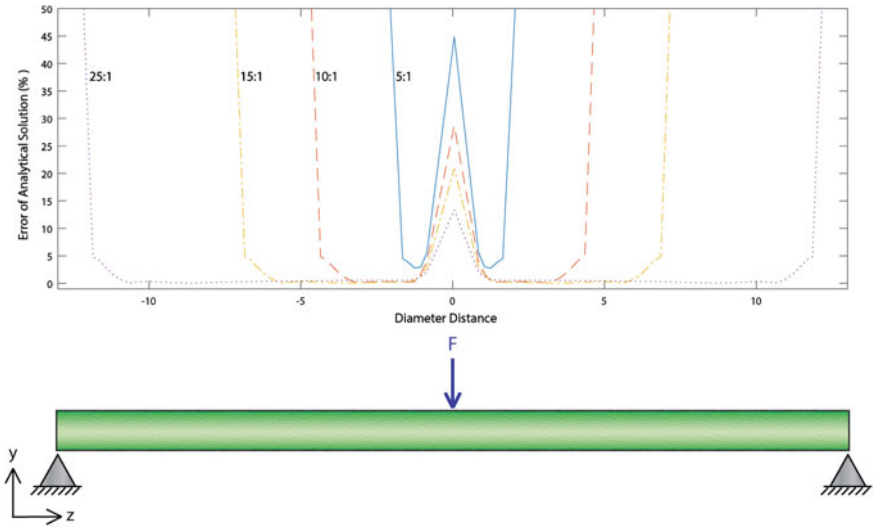

Fig. 9 Relative error of the analytic solution for σ_{zz} in hollow stem models having sample slenderness values of 25:1, 15:1, 10:1 and 5:1. All lengths are measured in number of diameters from the point of loading

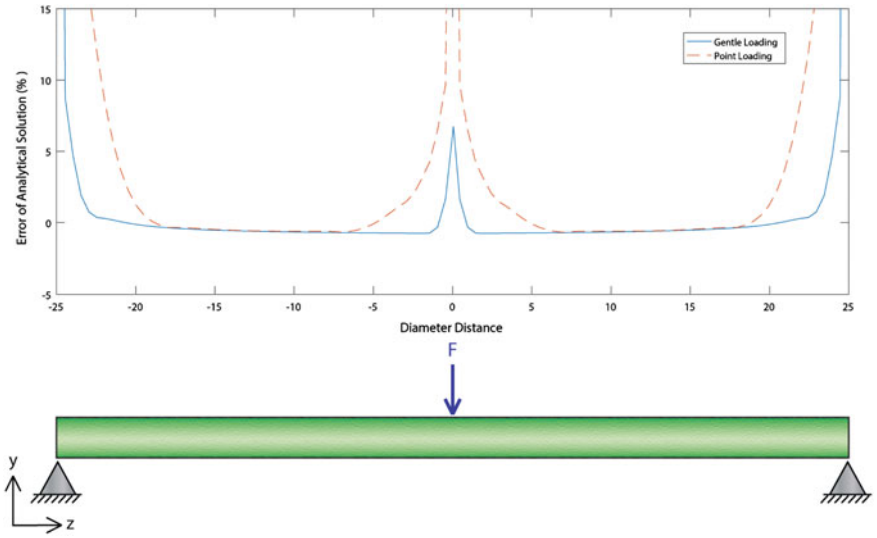

Fig. 10 Relative error of the analytic solution for σ_{zz} in a hollow stem model for gentle loading and point loading. All lengths are measured in number of diameters from the point of loading

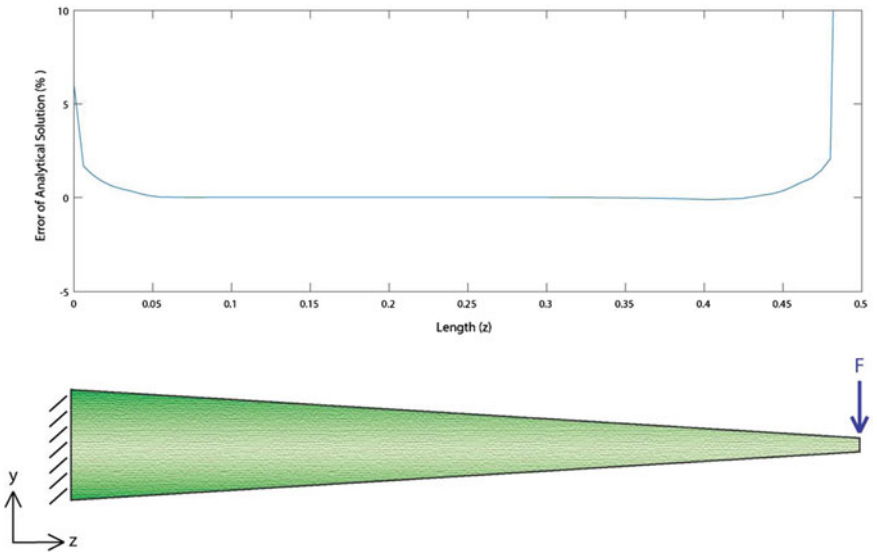

Fig. 11 Relative error of the analytic solution for σ_{zz} in a 10:1 tapered hollow stem model for cantilever point loading

for cross sections with nonconstant material stiffness or for two-material models (constant material properties within the two domains like rind and pith). The following figure shows stress distributions for rind–pith plant stems in which the rind

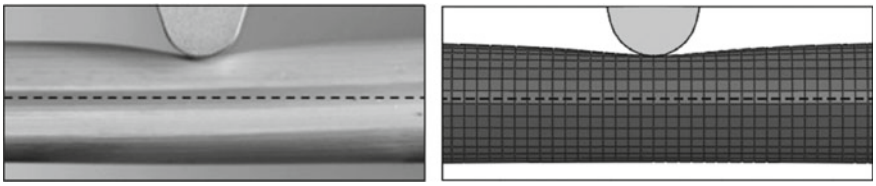

Fig. 12 Cross-sectional deformation caused by intermodal loading for (Robertson et al. 2015b) laboratory testing (left) and finite element solution (right)

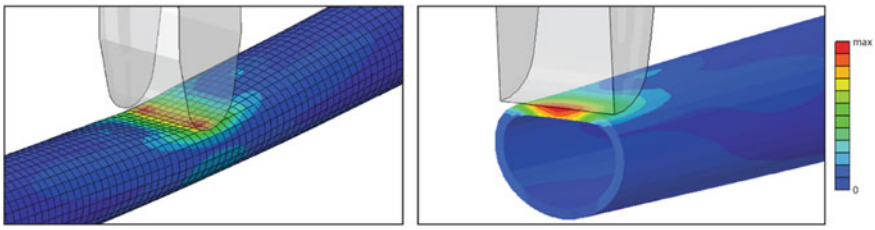

Fig. 13 Finite element model, depicting von Mises stresses for an isometric view (left) and a view cut through the center of the loading (right)

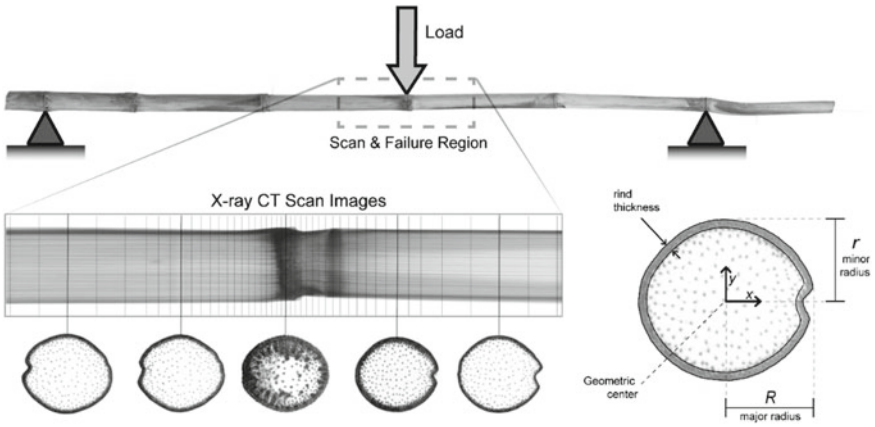

Fig. 14 Diagram depicting three-point bending test arrangement and region of CT scan (top), axial and transverse CT scan images (lower left), and an annotated cross section indicating some features identified through image processing (lower right)

is 20 times stiffer than the pith material. For such situations, Eq. 19 can be used to show that the ratio of stresses on either side of the pith/rind interface is exactly equal to the stiffness ratio across the interface. For the case shown below, σ_{zz} near the interface in the pith is 20x lower than the stresses in the rind. Equation 19 can also be used to assess stresses for continuously varying material stiffness, as shown later (see Fig. 16).

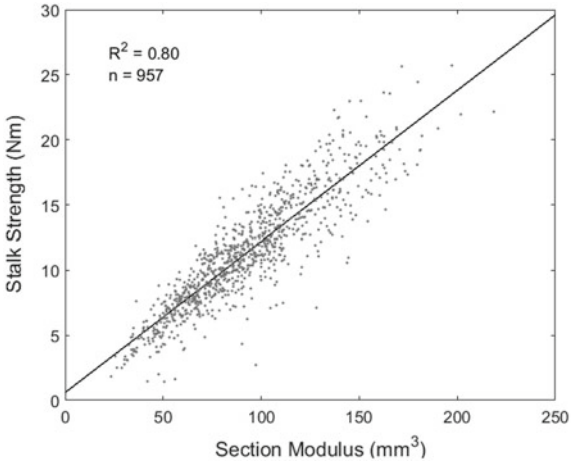

Fig. 15 Scatter plot and regression line between the stalk strength (maximum internal bending moment) and the section modulus of the rind

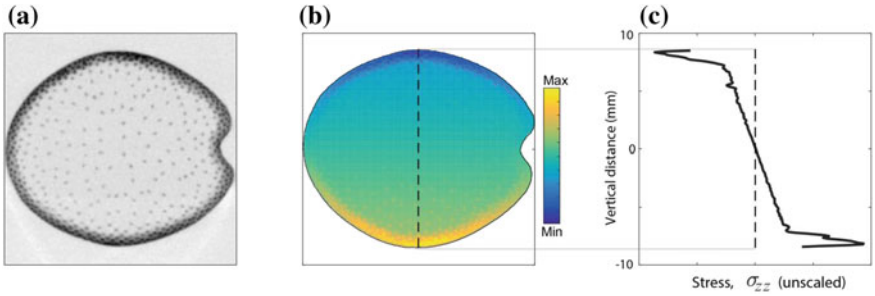

Fig. 16 Left: CT cross-section image; Center: σ_{zz} as determined by Eq. 19; Right: A line plot of σ_{zz} along the dashed line in the center image

Assumptions (E) and (F): Constant Shear in the X Direction

Assumption (F) states that τ_{yz} is constant in the x direction. This assumption is valid for rectangular cross sections in which there is no geometric or material variation along x direction, but it is not necessarily valid for cross sections that do not meet these criteria.

Figure 7 shows the distribution of τ_{yz} for hollow and solid circular cross sections. While the analytic bending equations generate horizontal bands of shear stress, the finite element model does not. This is because the circular geometry results in distributions of τ_{yz} that differ from the Assumption F. It should be noted that this model uses uniform cross-sectional stiffness. Stiffness variation in the cross section, which is common in plant stems would likely cause even further deviation from this assumption.

Assumption E is that two shear components can be neglected ($\tau_{xy} = \tau_{xz} = 0$). As shown in Fig. 3, although τ_{xy} is negligible, τ_{xz} is comparable in magnitude to τ_{yz}. Figure 8 shows that this shear component is zero in the analytic model, but not in the finite element model.

As seen in Figs. 7 and 8, the analytic bending equations do not accurately predict shear stresses. However, these inaccuracies may not be severe limitations for the prediction of failure. Recall that σ_{zz} is generally much larger than either stress component, and that the discrepancy between normal and shear stresses decreases with increasing distance from an applied load or a support. This is because stress formulations such as principal stress, maximum shear stress, and von Mises stress tend to amplify the influence of σ_{zz} (see Eqs. 22, 23, and 25). In addition, maximum σ_{zz} occurs at the top center and bottom center of the cross section, but shear stress components are very small at these points. As a result, analytic bending equations tend to be quite accurate, as will be discussed in the following section.

Structural Characteristics of Plant Stems

This section addresses aspects of plant stems that are not typically addressed in traditional mechanics textbooks, such as orthotropy, error as a function of diameter distance, sample slenderness, inhomogeneity, taper, and loading effects. The influence of each of these factors on the accuracy of bending stress equations is discussed below.

Orthotropy

Orthotropic materials are those in which material properties are orthogonal to each other (Nagarajan and Zak 1985). Wood is a common example of an orthotropic material. Wood typically has one stiffness in the longitudinal direction, another stiffness in the radial direction, and yet another stiffness in the circumferential direction.

Derivations of bending stress equations in textbooks vary in their treatment of orthotropy. Introductory level textbooks generally do not address this issue. As shown above, equations for bending stress (Eqs. 10 and 19) are valid for orthotropic materials (Hashin 1968; Silverman 1964). Thus, the primary material property for modeling bending stresses within plant stems is the longitudinal elastic stiffness or longitudinal Young's modulus, E_z.

Assumptions About the Stem Cross Section

The derivation of bending stress equations was made without restrictions on cross-sectional geometry. Finite element results provided above show that the analytic equations are reliable for both hollow and solid cross sections. However, loads that do not pass through the shear center of a beam induce torsional stresses in addition to bending stress (Boresi and Schmidt 2003). Thus, the equations above should only be applied when loading is aligned with the shear center of a stem. The determination of the shear center is beyond the scope of this chapter, but for circular and elliptical stems with symmetrical or axisymmetrical material properties, the shear center is collocated with the geometric center of the stem.

Most textbook derivations of bending stress equations assume a homogeneous cross-section. While this may be a reasonable approximation for woody stems, most plant stems exhibit some spatial variation in cross-sectional stiffness (Niklas 1992). Equations 16–21 show how the traditional equations can be modified to account for variation in cross-sectional stiffness. Figures 4, 6, 7 and 8 show distributions for the analytical and finite element models for various cross sections relevant to plant stems. In most cases, the bending equations provide relatively good estimates of stress.

Slenderness

Many sources indicate the accuracy of the bending stress equations is related to sample slenderness, defined as the ratio of length to diameter (*L/D*) of the sample (Boresi and Schmidt 2003; Niklas and Spatz 2012). This is not completely correct. The accuracy of the analytic equations is primarily dependent upon *diameter distance*. This is illustrated in Fig. 9, which contains data for several hollow stem models, each having a different sample slenderness. Observe that the accuracy of the analytic model at a diameter distance of 3 is identical for models of varying sample slenderness. Model accuracy is, therefore, highly dependent upon diameter distance, but only weakly dependent on sample slenderness.

Errors in Fig. 9 above 1–2% are due to the complex stress states that exist near loading points. These complex stresses cannot be predicted by the analytic model because several stress components have been neglected (Assumptions B and E). However, the finite element can predict stress and deformation near a loading point. Similar studies can be found in the engineering field that demonstrates the limitations of the elementary analytical equations to predict stresses near the loading points and boundary conditions (Sandorff 1980; Sullivan and Van Oene 1986; Williams 1989; Yu 1973).

Loading Effects

The analytic bending equations do not capture the complex stress states that occur near applied loads. Within the finite element method, similar loading conditions can be specified in a number of ways. Figure 9 was generated with distributed loading configurations that most closely mimic the analytical model. However, these boundary conditions underestimate loading effects. An alternative involves applying loads and supports at individual points within the finite element model, which tends to overestimate loading effects. Figure 10 shows curves for both gentle and point loading cases, illustrating the range of possible loading effects. The finite element model used to generate this figure was a hollow model with a rind thickness that was 15% of the radius. Because hollow stems are most susceptible to loading effects, the "Point Loading" curve in Fig. 10 is a reasonable "worst-case scenario" for bending in plant stems. For distances of 5 diameters from any loading point, the analytical model has an error of less 1%. Similar studies were conducted to assess the loading effects on the orthotropic beams under concentrated loads pointing toward considerable departure from classical beam theory (Sandorff 1980; Sullivan and van Oene 1986; Whitney 1985).

Taper

Plant stems are often tapered, but traditional derivations of bending equations often state an assumption of constant cross-sectional geometry (Beer et al. 2012; Crandall 2012; Niklas 1992; Timoshenko 1940). The derivation presented in this chapter does not make use of any assumptions about cross-sectional variation. However, the derivation does assume that the stress state is such that σ_{zz} is much larger than any other components (Assumption B). While abrupt variations in cross-sectional area will activate σ_{xx} and σ_{yy} stress components, gradual taper generally will not violate this assumption.

Figure 11 depicts the σ_{zz} predictions for a tapered (10:1), hollow plant stem. In this figure, the diameter decreases by one unit for every 10 units of length along the stem, as shown in the diagram below the chart. A relatively moderate taper actually provides a fairly accurate prediction of internal stresses. Excluding end effects, the finite element model is within 1% of the analytical solution. The effect of taper is addressed further in the following case study.

In general, gradual variation in stem properties is accurately predicted by the bending stress equations (Maki and Kuenzi 1965; Shahba et al. 2013). This is true for gradual changes in shape as well as material properties. However, rapid changes in shape and/or stiffness may not be predicted accurately.

Case Studies

This section provides an experimental perspective on the equations and results presented above. Laboratory testing of maize stems in three-point bending are described and the bending stress equations are used to aid in interpreting the experimental data.

A number of studies have investigated the strength of maize stem using three-point bending studies (Davis and Crane 1976; Robertson et al. 2014, 2015b; Tongdi et al. 2011). However, in a number of these studies, the load was applied at the internode. It was recently demonstrated that transverse loads, when applied at internode locations, cause deformation of the cross section, leading to premature failure (Robertson et al. 2015b, 2016; Tongdi et al. 2011). As mentioned above, bending equations cannot be trusted to produce accurate predictions of internal stresses at loading points.

When transverse loads are applied to a non-solid (i.e., hollow or pith-filled) plant stem, significant transverse deformation of the stem cross section can occur. This is depicted both experimentally and computationally in Fig. 12. A more detailed depiction of the deformation and stresses that result from this loading configuration are shown in Fig. 13. Robertson et al. recommended that loads and support points should be located at the nodes, and that the overall stem length should be maximized (Robertson et al. 2014, 2015b). Node-loading reduces transverse deformation, while the longer stem length reduces the transverse load required to achieve a given internal bending moment.

The node-loading approach was applied to a set of 1000 maize stems to determine the connection between stem morphology and strength (Robertson et al. 2015a, 2016). X-ray computed tomography was used to obtain three-dimensional images of maize stems. After imaging, the stems were tested in three-point bending. Displacement was increased and the applied load was measured until failure of the stem occurred.

Image processing techniques were used to extract various features of the stem morphology from X-ray CT data. This information was used to calculate the area moment of inertia of the entire stem cross section, as well as the area moment of inertia of the pith region and the rind region. Each region was assumed to possess homogeneous material properties.

Because the rind tissue is the primary load-bearing component of the stem, the pith tissue was neglected. The rind tissue was assumed to be homogeneous (Assumption D). Equation 10 was rearranged as follows to model these stems:

$$M_{\max} = \sigma_{\max} \frac{I_{rind}}{y} = \sigma_{\max} S_{rind} \tag{26}$$

In the above equation, S is referred to as the section modulus. The term σ_{max} refers to the maximum tissue strength. Figure 15 shows the relationship between the section modulus of the rind (S_{rind}) and stem strength (M_{max}).

The slope of the curve fit line in Fig. 15 can be interpreted as representing the maximum tissue strength (Eq. 26). The slope of the line in Fig. 15 is 120 MPa, which represents the average value of maximum tissue strength for this sample. Individual

values of σ_{max} ranged from 28 to 210 MPa, which is within the range spanned by many species of wood (Gibson et al. 2010; Forest Products Society 2011). It should be noted that the use of Eq. 26 neglects the role of the pith. The tissue strength values should, therefore, be interpreted cautiously. Equation 19 would be a more appropriate choice, given the architecture of the maize stalk shown in Fig. 14. But that approach would require assessment of both rind and pith stiffnesses, which is relatively difficult.

Although rind and pith stiffnesses were not measured, an exploration of the stress distribution within the stem is still possible. In human biomechanics, the intensity of CT scans has been shown to be correlated to material stiffness (Zioupos and Currey 1998). In addition, X-ray absorption is closely related to density, and for plant tissues, density is often correlated with tissue stiffness (Gibson and Ashby 1999; Nakagawa et al. 1986). It is, therefore, reasonable to assume that pixel intensity of maize stems is correlated with tissue stiffness. With this assumption in place, Eq. 19 was used to obtain an estimate of the distribution of bending stresses within the maize cross section. This was accomplished by assuming (1) a linear relationship between CT intensity and tissue stiffness; (2) equal tissue stiffness in tension and compression; and (3) the neutral layer coincident with the geometric center of the cross section. Figure 16 shows one CT cross section and an estimate of the σ_{zz} distribution within the cross section.

It should be noted that the stresses in the above figure are qualitative rather than quantitative. Because the mapping between CT intensity and material stiffness is not well defined, this approach provides the shape of stress distributions rather than stress magnitudes.

Nevertheless, this analysis can provide some interesting insights. First, although the pith is composed of parenchyma and vascular bundles, it generally seems to act as a nearly homogeneous material. Second, an assessment of the percentage of total internal bending moment supported by the pith versus the rind can be performed. For this cross section, the rind was measured using an image processing algorithm (Robertson et al. 2016) and the stresses within the pith and rind were assessed separately. The average stiffness of the rind was assumed to be 20 times higher than the average stiffness of the pith. Under this assumption, the rind provided 87% of the total internal bending moment supported by the cross section, with the pith providing the remaining 13% of support. Third, although stress is related to stiffness, strength and stiffness are different mechanical properties. Tissue failure will, therefore, occur whenever/wherever the local tissue stress exceeds the local tissue strength, which may not be in regions of highest stress. Finally, examination of model results often raises new questions. For example, the line graph above indicates that the highest stresses are developed just inside the outer surface of the stem. But for models with a homogeneous rind, the highest stresses are developed at the outer surface. There may be structural advantages when highest stresses are interior rather than at the surface. On the other hand, this result may be due to limitations in CT technology. Boundaries are never exact in CT images but are often blurred. This blurring effect may artificially decrease CT pixel intensity and therefore decrease the calculated material stiffness near the edge of the stem thus lowering stresses. In either case, the

use of such models can generate research questions that may not have been asked without insights from model results.

Summary and Future Work

This chapter has provided a derivation of bending stress equations that take into consideration many issues that are relevant to modeling bending stresses in plant stems. It should be noted that bending stresses developed in response to external loads are in addition to internal stresses that may exist within the plant stem prior to the application of bending loads. The equations presented in this chapter, therefore, address stresses due to external loads only.

Although plant stems are complex structures, relatively few assumptions are required to obtain bending stress equations that are applicable to plant stems. Equations for stems with variation in cross-sectional stiffness were also developed. The assumptions used to develop these equations were examined and the results of these investigations should allow researchers to make well-informed decisions when modeling plant stems in this manner. The examination of additional issues such as diameter distance, sample slenderness, taper, and loading effects provided additional insights into issues that are of interest when modeling plant stems.

For easy reference, the most commonly used bending stress equations are presented in Table 3 along with their accompanying assumptions and notes regarding applications of the respective equations.

Future Work

Nodes in plant stems serve as mechanical bulkheads and, therefore, act to minimize cross-sectional ovalization which in turn increases bending stiffness (Robertson et al. 2015a; Schulgasser and Witztum 1992). Due to the complexities involved in creating realistic finite element models of stems with nodes, this issue was not investigated in this study. Based on the results shown in Fig. 15 and other studies, bending stress equations may be suitable in the presence of nodes. A more detailed analysis will be required to adequately address this issue.

The primary limitation of the bending equations appears to be the difficulty of assessing spatial variations in material properties. Without information about the distribution and value of material properties, only the traditional form of the bending stress equation can be used. This equation assumes a single material stiffness, which may be a rather crude assumption for many plant stems. Techniques for assessing spatial distribution of material properties would enable a much more detailed analysis of stress distributions within plant stems.

At the same time, it is not yet clear how the material properties of the pith and rind vary with moisture content. In a wet plant stem, water may actually play a

Table 3 Normal and shear stress equations with their accompanying assumptions and notes regarding application of these equations

	Assumptions required	Equation(s)	Notes
Normal stresses	A. Stress state is dominated by the normal stress σ_{zz} B. The material is linearly elastic C. Bending is locally approximated by an arc D. Material tissue is homogeneous in the cross section	$\sigma = \frac{My}{I}$	•Diameter distance > 5:1 typically ensures that assumptions A & C are valid •Material may be orthotropic •Not valid near loading points or in regions where the cross-sectional shape changes rapidly
	All of the above except D	$\sigma = \frac{M\,E(x,y)\,y}{I_E}$ $I_E = \int_A E(x,y)y^2 dA$	•Same notes as above •Captures stress variation due to cross-sectional variation in material stiffness
Shear stresses	Assumptions A—D and: A. τ_{yz} is constant in the x direction B. τ_{xy} and τ_{xz} are negligible	$\tau_{yz} = \frac{V(z)}{I\,w(y)} \int_{y_i}^{y_f} y\,dA$	•This assumption introduces errors when applied to non-rectangular cross sections
	Assumptions A—C and: E. τ_{yz} is constant in the x direction F. τ_{xy} and τ_{xz} are negligible	$\tau_{yz} = \frac{V(z)}{I_E\,w(y)} \int_{y_i}^{y_f} E(x,y)\,y\,dA$	•This assumption introduces errors when applied to non-rectangular cross sections
Combined stresses	The only significant stresses are σ_{zz} and τ_{yz}	$\sigma_1,\ \sigma_2 = \frac{\sigma_{zz}}{2} \pm \sqrt{\frac{\sigma_{zz}^2}{4} + \tau_{yz}^2}$ $\tau\text{max} = \sqrt{\frac{\sigma_{zz}^2}{4} + \tau_{yz}^2}$ $\sigma_v = \sqrt{\sigma_{zz}^2 + \frac{1}{3}\tau_{yz}^2}$	•For diameter distance values above 5, σ_{xx}, σ_{yy} τ_{xy}, and τ_{xz} are negligible

role in mechanical support (Niklas 1992).This is because the water is essentially incompressible—in a confined space it could potentially resist compression as well as tension (Crum 1979). More work is needed in order to determine the effect of water on bending strength of stems.

The lack of quantitative material properties is also a limitation for predicting other modes of failure. Equations for plant stem buckling have been provided by Spatz et al. (1990) and Schulgasser and Witztum (1992). Whereas bending stress depends upon just one material stiffness, buckling equations typically include several additional material properties, including transverse stiffness. Connecting these equations with experiments is very difficult due to limitations in assessing materials properties. Methods for assessing multiple material properties would enable a great deal of additional work on the mechanisms of stem failure.

In general, further progress in the prediction of plant stem failure is limited by a lack of methods for quickly assessing mechanical properties of plant samples. More research is needed in this area to support advances in plant biomechanics.

Acknowledgments This work was supported by funding from the National Science Foundation (Award #1400973), the United States Department of Agriculture (Award #2016-67012-24685) and the New York University Abu Dhabi Global Ph.D. Fellowship.

Finite Element Model Description

The finite element model used throughout this chapter was developed in Abaqus/CAE 16.4-1. The analysis consisted of a single part, meshed with three-dimensional continuum 20-noded full integration hexahedral elements, with the mesh densities as shown in the figures throughout the chapter. The material represents an average maize stem as described in (Von Forell et al. 2015). For the three-point bending analysis, half the length of the stem was modeled, with symmetry boundary conditions applied at the point of loading. For the gentle loading analyses, the load was applied through the entire cross section as a distributed traction pressure, and the simple support was modeled as constrained vertical deflection at the neutral layer nodes. For the point loading analysis, the load was applied at the top node as a point load, and the simple support was modeled as constrained vertical deflection at the bottom node. The model was run as a linear general static analysis, using a full Newton direct solver in Abaqus/Standard 6.14–1.

References

Agarwal BD, Broutman LJ, Chandrashekhara K (2006) Analysis and performance of fiber composites. Wiley, New York

Archer RR (1987) Internal residual stress patterns in tree stems. In: Growth stresses and strains in trees. Springer, pp 66–113

Bauchau O, Craig J (2009) Euler-bernoulli beam theory. In: Structural analysis. Springer, pp 173–221

Beer F Jr, Russell Johnston E, DeWolf J, Mazurek D (2012) Mechanics of materials. McGraw-Hill, New York

Boresi A, Schmidt R (2003) Advanced mechanics of materials. Wiley, New York

Byars EF, Snyder RD, Plants HL (1983) Engineering mechanics of deformable bodies. Harpercollins College Div

Callister WD, Rethwisch DG (2012) Fundamentals of materials science and engineering: an integrated approach. Wiley, New York

Coutand C, Julien J, Moulia B, Mauget J, Guitard D (2000) Biomechanical study of the effect of a controlled bending on tomato stem elongation: global mechanical analysis. J Exp Bot 51(352):1813–1824

Crandall SH (2012) An introduction to mechanics of solids. Tata McGraw-Hill Education, New York

Crum LA (1979) Tensile strength of water. Nature 278(5700):148–149

Davis SM, Crane PL (1976) Recurrent selection for rind thickness in maize and its relationship with yield, lodging, and other plant characteristics. Crop Sci 16(1):53–55

Dean T, Long JN (1986) Validity of constant-stress and elastic-instability principles of stem formation in pinus contorta and trifolium pratense. Ann Bot 58(6):833–840

Forest Products Society (2011) Wood Handbook: Wood as an engineering material
Gibson Lorna J et al. (2010) Cellular materials in nature and medicine. Cambridge University Press
Gibson LJ (2012) The hierarchical structure and mechanics of plant materials. J R Soc Interface:rsif20120341
Gibson LJ, Ashby MF (1999) Cellular solids: structure and properties. Cambridge University Press, New York
Hashin Z (1968) Erratum: "plane anisotropic beams" (journal of applied mechanics, 1967, 34, pp 257–262). J Appl Mech 35 (3):623–623
Kim N-H, Sankar BV (2009) Introduction to finite element analysis and design. Wiley, New York
Kokubo A, Kuraishi S, Sakurai N (1989) Culm strength of barley correlation among maximum bending stress, cell wall dimensions, and cellulose content. Plant Physiol 91(3):876–882
Maki A, Kuenzi EW (1965) Deflection and stresses of tapered wood beams
Nagarajan S, Zak AR (1985) Finite element model for orthotropic beams. Comput Struct 20(1–3):443–449
Nakagawa F, Kobayashi S, Takemae T, Sugita K (1986) Aneurysms protruding from the dorsal wall of the internal carotid artery. J Neurosurg 65(3):303–308
Niklas KJ (1992) Plant biomechanics: an engineering approach to plant form and function. University of Chicago press, Chicago
Niklas KJ, Spatz H-C (2012) Plant physics. University of Chicago Press, Chicago
Riley WF, Zachary LW (1989) Introduction to mechanics of materials. Wiley, New York
Robertson D, Smith S, Gardunia B, Cook D (2014) An improved method for accurate phenotyping of corn stalk strength. Crop Sci 54(5):2038–2044
Robertson DJ, Julias M, Gardunia BW, Barten T, Cook DD (2015a) Corn stalk lodging: a forensic engineering approach provides insights into failure patterns and mechanisms. Crop Sci 55(6):2833–2841
Robertson DJ, Lee SY, Julias M, Cook DD (2016) Maize stalk lodging: flexural stiffness predicts strength. Crop Sci 56(4):1711–1718
Robertson DJ, Smith SL, Cook DD (2015b) On measuring the bending strength of septate grass stems. Am J Bot 102(1):5–11
Rüggeberg M, Speck T, Paris O, Lapierre C, Pollet B, Koch G, Burgert I (2008) Stiffness gradients in vascular bundles of the palm washingtonia robusta. Proc R Soc Lond B Biol Sci 275(1648):2221–2229
Sandorff PE (1980) Saint-venant effects in an orthotropic beam. J Compos Mater 14(3):199–212
Schulgasser K, Witztum A (1992) On the strength, stiffness and stability of tubular plant stems and leaves. J Theor Biol 155(4):497–515
Shahba A, Attarnejad R, Hajilar S (2013) A mechanical-based solution for axially functionally graded tapered euler-bernoulli beams. Mech Adv Mater Struct 20(8):696–707
Shukla A, Agarwal B, Bhushan B (1989) Determination of stress intensity factor in orthotropic composite materials using strain gages. Eng Fract Mech 32(3):469–477
Silverman IK (1964) Orthotropic beams under polynomial loads. J Eng Mech Div 90(5):293–320
Spatz H, Speck T, Vogellehner D (1990) Contributions to the biomechanics of plants. ii. Stability against local buckling in hollow plant stems. Plant Biol 103(1):123–130
Speck T, Burgert I (2011) Plant stems: Functional design and mechanics. Annu Rev Mater Res 41:169–193
Speck T, Spatz H, Vogellehner D (1990) Contributions to the biomechanics of plants. I. Stabilities of plant stems with strengthening elements of different cross-sections against weight and wind forces. Botanica Acta 103 (1):111–122
Sullivan J, Van Oene H (1986) An elasticity analysis for the generally and specially orthotropic beams subjected to concentrated loads. Compos Sci Technol 27(2):133–155
Timoshenko S (1940) Strength of materials. D. Van Nostrand Company Incorporated, New York
Tongdi Q, Yaoming L, Jin C (2011) Experimental study on flexural mechanical properties of corn stalks. In: 2011 international conference on new technology of agricultural engineering (ICAE). IEEE, pp 130–134

Vandiver R, Goriely A (2009) Differential growth and residual stress in cylindrical elastic structures. Philos Trans R Soc Lond A Math Phys Eng Sci 367(1902):3607–3630
Von Forell G, Robertson D, Lee SY, Cook DD (2015) Preventing lodging in bioenergy crops: a biomechanical analysis of maize stalks suggests a new approach. J Exp Bot 4367–4371
Wegst UG, Ashby MF (2007) The structural efficiency of orthotropic stalks, stems and tubes. J Mater Sci 42(21):9005–9014
Whitney JM (1985) Elasticity analysis of orthotropic beams under concentrated loads. Compos Sci Technol 22(3):167–184
Williams J (1989) End corrections for orthotropic dcb specimens. Compos Sci Technol 35(4):367–376
Wood Handbook: Wood as an Engineering Material. Forest Products Society, (2011)
Yu JC (1973) Local effects of a concentrated load applied to orthotropic beams. J Franklin Inst 296(3):191–206
Zandomeni K, Schopfer P (1994) Mechanosensory microtubule reorientation in the epidermis of maize coleoptiles subjected to bending stress. Protoplasma 182(3–4):96–101
Zioupos P, Currey J (1998) Changes in the stiffness, strength, and toughness of human cortical bone with age. Bone 22(1):57–66